Biomedical Applications of Smart Polyurethane Bionanocomposites

Ricci A.L. & Ibrahim T.K.

Department of Cardiovascular Sciences, Pisa Medical Academy, Pisa, Italy

Department of Clinical Cardiology, Abu Dhabi Health Institute, Abu Dhabi, UAE

ABSTRACT

Thermo- and magneto-responsive shape-memory bionanocomposites based on a bio-based polyurethane and magnetite nanoparticles were prepared. Due to the structure of the reactants, the behavior of the polyurethane matrix differs from common polyurethanes, since the soft segment was formed by a diisocyanate and a chain extender, whereas the macrodiol served as hard segment. The influence of the magnetite nanoparticles on the thermal and mechanical properties and the shape-memory behavior was studied. It was observed that magnetite nanoparticles interacted with macrodiol-rich domains and decreased the overall crystallinity of the material, although their presence did not affect the mechanical properties to a great extent. At the same time, the magnetite nanoparticles increased the shape fixity and contributed to shape recovery. The bionanocomposites exhibited magnetic behavior and could be easily heated in an alternating magnetic field, allowing fast and almost complete shape recovery. Preliminary cytotoxicity, hemocompatibility, and cell adhesion analysis suggest that the new materials are benign and potentially useful for biomedical applications.

Keywords: Bionanocomposites, bio-based polyurethane, magnetite nanoparticles, shape-memory, magneto-responsive, biocompatibility.

INTRODUCTION

Shape-memory polymers (SMPs) have gained significant attention among the scientific community in the last decade since they are possibly useful for a wide range of applications in different industries.[1–3] Moreover, if compared with other shape-memory materials such as ceramics or alloys, SMPs show technical advantages due to their good recovery, low density, low cost and ease in processing and in tailoring their properties just by changing their composition.[2,4] SMPs can be deformed to and fixed in a temporary shape and recover their original shape in response to an external stimulus such as heat, magnetic or electric fields, exposure to moisture, a change of the pH, irradiation with light, and other stimuli.[5,6] Most of the reported SMPs are thermo-

responsive and shape recovery is triggered by direct heating. SMPs are obtained by combining a physically or chemically cross-linked network structure that offers rubber elasticity and a switching element, i.e., a second type of cross-links that can be switched on or off with an external stimulus. This element, which is responsible for the shape fixity, is often created by way of phase separation, and a phase transition temperature (T_{trans}), which can either be a glass transition (T_g) or a melting temperature (T_m), is used as the switch. During the programming, the material is heated and deformed at a switching temperature (T_s) above T_{trans} and is subsequently cooled below T_{trans} in order to fix the temporary shape. The original shape is restored when the sample is reheated above T_{trans}.[7,8] In some applications, such as in certain biomedical applications, the shape memory objects cannot be heated directly and the shape recovery has to be triggered using an indirect method. This can be achieved by the incorporation of magnetic nanoparticles, applying an alternating magnetic field, and converting electromagnetic radiation into heat.[9]

Segmented thermoplastic polyurethanes (STPUs) represent a widely investigated SMP platform, since their chemical structure can readily be varied, allowing to access elastomers whose properties cover a wide range.[10–12] Moreover, many STPUs are physiologically benign and thus useful for biomedical applications.[3,13–15] STPUs are block polymers consisting of two segments, one of which is a macrodiol and the other is formed by the reaction of a diisocyanate and a low-molecular-weight chain extender. The incompatibility between the two segments leads to microphase separation, the extent of which is strongly dependent on the chemical composition and the length of the blocks.[16,17] In recent years, monomers derived from renewable sources such as vegetable oils, amino acids, and polysaccharides are increasingly being used in the synthesis of STPUs with the goal of reducing the use of monomers derived from fossil sources and their adverse impact on the environment.[18,19] In this context, it was observed in a previous study[10] that the combination of an aliphatic asymmetric bio-based diisocyanate (L-lysine diisocyanate, LDI) and a diol chain extender derived from corn sugar (1,3-propanediol, PD) afforded an amorphous phase which is not able to form crystalline domains with a T_g that is much lower than T_m of the crystalline domains formed by a macrodiol derived from castor oil. This peculiar behavior led to an “inversion” of the role of the phases. Whereas in common thermo-responsive shape-memory polyurethanes the phase formed by the macrodiol is used as the switching element, while the phase constituted by the diisocyanate and chain extender serves as permanent cross-links,[20,21] here the macrodiol-rich domains acted as the hard phase.

SMPs can be loaded with different nano-fillers, such as chitin, cellulose and magnetite nanoparticles (MNPs) in order to modify their shape-memory properties and/or to impart responsiveness towards a specific stimulus.[9,22–26] The incorporation of MNPs allows inducing heat to the material by the application of an alternating magnetic field (AMF). In this way, the shape recovery of the material could be triggered without direct contact with a thermal source.[9,27,28]

Combining these approaches, we here report thermo- and magneto-responsive shape-memory bionanocomposites based on a fully bio-based polyurethane synthesized from a macrodiol derived from castor oil, L-lysine diisocyanate, and bio-based 1,3-propanediol that were loaded with different amounts of MNPs. Thin films were prepared by solvent-casting and the thermal, mechanical, and shape-memory properties of the new bionanocomposites were analyzed using differential scanning calorimetry (DSC), dynamic mechanical analysis (DMA), tensile testing, as well as cyclic shape-memory experiments. Moreover, the magneto-response of the bionanocomposites was studied by applying an alternating magnetic field. Finally, biocompatibility was assessed by performing cytotoxicity, hemocompatibility and cell adhesion assays.

EXPERIMENTAL

Materials

To synthesize the MNPs, iron (III) chloride hexahydrate (98%) (Panreac), iron (II) chloride tetrahydrate (≥ 99%) (Sigma-Aldrich), ammonium hydroxide (30%) (Panreac), and oleic acid (90%) (Fluka) were used. Tetrahydrofuran (THF) (HPLC grade) supplied by Macron Fine Chemicals was employed to disperse the MNPs, and also as solvent for the preparation of the bionanocomposites by solvent-casting. The polyurethane matrix was synthesized using a macrodiol derived from castor oil (poly(butylene sebacate)diol), ethyl ester L-lysine diisocyanate (LDI) (226 g mol^{-1}) (CHEMOS GmBH) and a chain extender derived from corn sugar, 1,3-propanediol (PD) (76 g mol^{-1}) (Quimidroga S.A.). The hydroxyl index of the macrodiol was 32.01 mg KOH g^{-1}, determined by titration based on ASTM D 4274-88 Test Method A standard, and a number-average molecular weight of 3505 g mol^{-1}. The macrodiol, LDI and PD have bio-based carbon contents of 72, 81 and 100%, respectively, as determined by a standard procedure according to ASTM-D6866. The chemical structures of the macrodiol, diisocyanate and chain extender are shown in Figure 1a.

a)

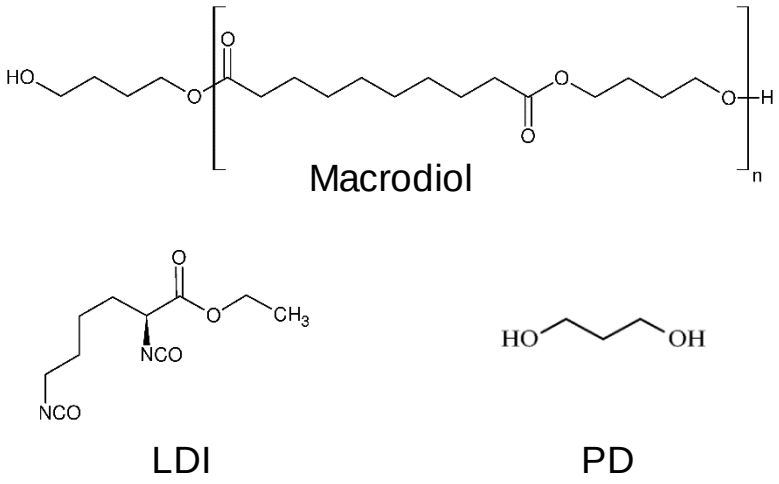

b)

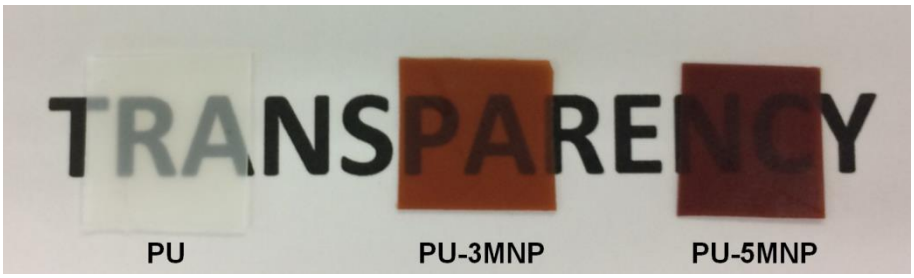

Figure 1. a) Chemical structure of the reactants employed for the synthesis of the biobased polyurethane matrix. b) Digital image of films of the neat PU and nanocomposites with 3 or 5 wt% MNPs.

For biocompatibility studies, L929 murine fibroblast obtained from ATCC (American Type Culture Collection) were used. The cells were cultured in Minimum Essential Medium (MEM), supplemented with 1 mM sodium pyruvate, 1% non-essential amino acids (Gibco, Paisley, UK), 1% penicillin-streptomycin (Lonza, Verviers, Belgium), and 10% fetal bovine serum (FBS; Biochrom AG, Berlin, Germany).

Preparation of magnetite nanoparticles

The MNPs were prepared by a co-precipitation method from an aqueous Fe^{3+}/Fe^{2+} solution (molar ratio 3:2) using ammonium hydroxide (30%) in excess. First, 0.09 molof $FeCl_3 \cdot 6H_2O$ and 0.06 mol of $FeCl_2 \cdot 4H_2O$ were dissolved in 50 mL of distilled water and the solution was heated to 70 °C. Subsequently, 40 mL of NH_4OH were added, which caused the immediate formation of a black precipitate. The particles were subsequently coated by adding 0.02 mol of oleic acid and the suspension was stirred at 80 °C for 30 min. The oleic acid coated MNPs thus obtained were washed with distilled water and

separated by centrifugation. The water was replaced and the centrifugation/washing cycle was repeated several times until a neutral pH was reached. After another centrifugation step, they were dispersed in THF and stored in a refrigerator at 4 °C. The concentration of the MNPs in THF was 4 g L^{-1}.

Synthesis of thermoplastic bio-based polyurethane

For the synthesis of the thermoplastic bio-based polyurethane matrix, a macrodiol derived from castor oil (poly(butylene sebacate)diol), a L-lysine amino acid based diisocyanate (ethyl ester L-lysine diisocyanate (LDI)), and a chain extender from corn sugar (1,3 propanediol (PD)) were combined following a two-step bulk polymerization procedure.[10] Briefly, first the dried macrodiol was reacted with LDI at 100 ˚C for 4 h in order to obtain a prepolymer. Subsequently, the dried PD was added and stirred for 10 min. The resulting viscous liquid was poured into a mold at it was pressed at 100 ˚C at 50 bar for 10 h. Finally, the polyurethane was left to cool down to room temperature at 50 bar. The NCO/OH ratio was 1.01. The molar ratio of the three components, macrodiol:LDI:PD, was 1:5.05:4, resulting in a LDI-PD content of 29 wt%. Taking into account the bio-based carbon content and weight percentage of the components it was determined that the bio-based carbon content of the matrix was 75%. Furthermore, the weight and number average molecular weight, as well as, the polydispersity index of the bio-based polyurethane were 100000, 40000 and 2.5, respectively, as previously reported.[10] Its chemical structure was analyzed by performing proton nuclear magnetic resonance (^{1}H NMR) and Fourier transform infrared (FTIR) spectroscopy, which can be found in the Supplementary Information.

Preparation of the bio-based polyurethane bionanocomposites

Shape-memory bionanocomposites based on the synthesized bio-based polyurethane and the MNPs were prepared by solvent casting. Bionanocomposites of 1 g were prepared; to that end, the bio-based polyurethane was dissolved in THF (50 mg mL^{-1}) and different volumes of the MNPs dispersed in THF were added to the solution, in order to prepare bionanocomposites with 3 and 5 wt% of MNPs. Subsequently, the mixture was sonicated in a Sonoswiss SW3H sonication bath for 1 h with a cold water recirculation system. The dispersion was subsequently cast into a poly(tetrafluoroethylene) mold having a diameter of 7.5 cm, which was then placed in an oven at 70 °C for 20 h to remove the solvent. Finally, the obtained films were compression-molded twice in a hot press at 80 °C at 5 bar for 5 min. The final thickness of the films was around 0.2 mm. The bionanocomposites produced are coded PU-xMNP, where x refers to the weight percentage (wt%) of MNP added. Furthermore, a neat bio-based polyurethane was also

prepared following the same procedure, which was designated as PU. In Figure 1b a digital image of the prepared polyurethane matrix and its bionanocomposites is shown.

Characterization techniques

The morphology of the MNPs and the prepared bionanocomposites were determined by performing wide-angle X-ray diffraction (XRD) studies. The XRD patterns were collected by using a Philips X'pert PRO automatic diffractometer operating at 40 kV and 40 mA, in theta-theta configuration, secondary monochromator with Cu-Kα radiation (λ = 1.5418 Å) and a PIXcel solid state detector (active length in 2θ = 3.347°). A fixed divergence and antiscattering slit giving a constant volume of sample illumination were used.

Transmission electron microscopy (TEM) was used to analyze the morphology of the MNPs. TEM studies were carried out on a Philips SuperTwin CM200 operated at 200 kV. The instrument was equipped with LaB6 filament and EDAX EDS microanalysis system. For samples preparation, MNPs were diluted in THF for 5 min in an ultrasonic bath (JP Selecta Ultrasons H-D). Subsequently a drop of the suspension was spread onto a TEM copper grid (300 Mesh) covered by a carbon film followed by drying under vacuum.

The characteristic functional groups of the MNPs were identified by means of Fourier transform infrared spectroscopy (FTIR) using a Nicolet Nexus FTIR spectrometer. To that end, KBr pellets were prepared and the spectra were obtained after 64 scans in the range of 4000-400 cm^{-1} with a resolution of 4 cm^{-1}.

The thermal properties of the bionanocomposites were analyzed by means of differential scanning calorimetry (DSC) using a Mettler Toledo DSC822e. Samples with a weight between 5 and 10 mg were sealed in aluminum pans and heated from -75 to 100 °C at a rate of 20 °C min^{-1}, using N_2 as a purge gas (20 mL min^{-1}). The crystallization process was followed by cooling the samples from 100 to -75 °C at a rate of 10 °C min^{-1}. The inflection point of the heat capacity change observed was chosen to evaluate T_g, and the maximum of the endothermic peak and the area under the peak were used to determine T_m and the melting enthalpy (ΔH_m). Similarly, the crystallization temperature (T_c) was determined from the minimum of the exothermic peak observed in the cooling scan and the crystallization enthalpy (ΔH_c) from the peak area. The ΔH_m and ΔH_c values are based on the total sample weight.

Based on the melting or crystallization enthalpy values, equation 1 was used to calculate the relative crystallinity of the bionanocomposites (χ_c) in the first heating ($\chi_{c\ heating}$) and cooling ($\chi_{c\ cooling}$) scans:[29]

$$\chi_c = \frac{\Delta H_{bc}}{\omega\ \Delta H_{100}} \qquad (1)$$

where ΔH_{bc} is the experimental melting or crystallization enthalpy value of the bionanocomposite, ω is the weight fraction of the neat bio-based polyurethane in the bionanocomposites and ΔH_{100} is the melting or crystallization enthalpy value of the matrix.

The dynamic mechanical behavior of the prepared bionanocomposites was analyzed by dynamic mechanical analysis (DMA) in tensile mode on an Eplexor 100N analyzer from Gabo, using a static strain of 0.10%. The temperature was varied from -100 to 75 °C at a scanning rate of 2 °C·min^{-1} and at a fixed operation frequency of 10 Hz. Samples were cut in strips of 22 mm x 5 mm x 0.2 mm.

Mechanical testing was carried out at room temperature using a Universal Testing Machine (UTM) (MTS Insight 10) with a load cell of 250 N and pneumatic grips. Samples were cut into strip shape (22 mm x 5 mm x 0.2 mm). Tests were performed with a crosshead rate of 50 mm min^{-1}. Elastic modulus (E), tensile strength at yield (σ_y), tensile strength at break (σ_b), strain at yield (ε_y) and strain at break (ε_b) were averaged from the data of at least five samples.

The thermally activated shape-memory properties were studied using an MTS Insight 10 instrument with a temperature chamber (Thermcraft). Strip shape samples of 22 mm x 5 mm x 0.2 mm were heated to the switching temperature (T_s) of 40 ºC for 10 min. Thereafter, samples were stretched up to 50% at a rate of 5 mm min^{-1}. Once the target strain was reached, samples were cooled under applied stress around to -10 ºC, which is below the transition temperature (T_{trans}) with a cooling spray (Freezer 5320, Jelt) to fix the temporary shape for 1 min and the applied stress was removed. The permanent shape was recovered upon heating the samples up to the switching temperature for 10 min. Five thermo-mechanical cyclic tensile tests were consecutively performed. Thermally activated shape-memory behavior was quantified taking into account the commonly used parameters, i.e. shape fixity (R_f) and shape recovery (R_r) values, which can be calculated using equations 2 and 3, respectively:

$$R_f(N) = \frac{\varepsilon_u(N)}{\varepsilon_m(N)} \cdot 100 \quad (2)$$

$$R_r(N) = \frac{\varepsilon_m(N) - \varepsilon_p(N)}{\varepsilon_m(N) - \varepsilon_p(N-1)} \cdot 100 \quad (3)$$

where ε_m is the maximum strain in the tensile test, ε_u is the residual strain after cooling below T_{trans} and unloading, ε_p is the residual strain after the shape recovery, and N is the number of cycles.

Magnetic measurements

The nanocomposites were tested in an alternating magnetic field (AMF) using a commercially available device (Magnetherm V1.5, Nanotherics Ltd.) equipped with a nine-turn solenoid operating at 523.5 kHz and 15.9 kA/m. The surface temperature of the nanocomposites during the AMF stimulation was monitored using a IR camera (Optris PI450, Optris GmbH). To trigger magnetically induced shape-memory effect, a Power Cube 32/1800 HF2 device operating with 1018KHz high-frequency generator, magnetic flux density of 21mT and coil diameter of 4mm was used.

Biocompatibility studies

Finally, the biocompatibility of the prepared bionanocomposites was analyzed by performing cytotoxicity, hemocompatibility and cell adhesion assays. For cytotoxicity and hemocompatibility, the extractive media was obtained by incubation of the material in complete medium (24 h) or phosphate buffered saline (1xPBS) (72 h) at 37 ºC, respectively. Every assay was performed according to ISO 10993-12:2007 standard.[30]

Cytotoxicity was assessed by PrestoBlue® (Invitrogen, USA), a resazurin-based solution that functions as a colorimetric cell viability indicator. For this assay, murine fibroblasts (L929 cells) were seeded into 96-well plates at a density of $4x10^3$ cells/well in 100 µL of complete culture medium. After 24 h, the medium was replaced with 100 µL of negative control, high-density polyethylene (HDPE) (complete medium), positive control, polyvinyl chloride (PVC) (DMSO, 10% in complete medium) or biomaterial´s extractive media. The optical density (OD) was measured at 570 and 600 nm in a spectrophotometer (Synergy HT spectrophotometer, Biotek, USA) at different time points (0, 24, 48 and 72 h). The viability of the cells was calculated from equation 4:

$$\text{Viability (\%)} = \frac{OD_{sample}}{OD_{negative\ control}} \cdot 100 \quad (4)$$

where OD_{sample} is the absorbance of the sample and positive control cells and $OD_{negative\ control}$ is the absorbance of the negative control cells. All assays were conducted in triplicate and average values and their standard deviations are reported.

Hemocompatibility was analyzed using the method of cyanomethemoglobin following ISO 10993-4:2009.[31] This colorimetric method is based on the principle that hemolysis of red cells lead to the release of hemoglobin, which can be converted to cyanomethemoglobin using ferricyanide in presence of bicarbonate, the cyanomethemoglobin formed can be quantified by measuring its absorbance at 540 nm.[32] For the hemocompatibility determination, blood samples were obtained from three different healthy donors and treated with Li–heparin to avoid coagulation. A pool of the three samples with plasma free hemoglobin (PFH) concentration below 1.0 mg mL^{-1} was used in the assay. First, pooled blood was diluted with 1 x PBS to adjust the total blood hemoglobin (TBH) concentration to 10 mg mL^{-1} (TBHd). Then, to assess the potential hemolytic effect of the bionanocomposite, 100 µL of sample extracted media and controls (positive control, 1% Triton X-100; negative control, 40% polyethylene glycol solution) were mixed with 100 µL of TBHd and 700 µL of 1 x PBS. The samples were incubated for 3 h at 37 °C and centrifuged for 15 min at 800 g. After that, the hemoglobin concentration of the sample supernatant was calculated according to cyanomethemoglobin standard curve at 540 nm in a microplate reader. The percentage of hemolysis was calculated according equation 5:

$$\text{Hemolysis (\%)} = \frac{\text{sample hemoglobin concentration - negative control concentration}}{\text{positive control concentration - negative control concentration}} \cdot 100 \quad (5)$$

The adhesion and morphology of the L929 cells on the surface of the materials was studied by scanning electron microscopy (SEM). The material was placed in 24-well ultra-low attachment plate and L929 were seeded onto it at a density of 1 x 10^5 cells cm^{-2}. SEM was carried out at 24, 48 and 72 h. At each time point, the sample was rinsed three times in Sorensen buffer (Panreac AppliChem, Spain), fixed using 2% glutaraldehyde (Panreac) in 0.1 M cacodylate buffer and post-fixed in 1% OsO_4 for 1 h, washed with PBS, dehydrated using a series of graded ethanol solutions and dried in hexamethyldisilazane for 10 min. The sample was then sputtered with a thin layer of gold under an argon atmosphere and observed using a Hitachi S-4800 scanning electron microscope with an accelerating voltage of 15 kV.

RESULTS AND DISCUSSION

The crystal structure and crystal size of the MNPs was determined by wide-angle X-ray diffraction (XRD). As can be observed in Figure 2a, the diffractogram of the MNPs show peaks at (220), (311), (400), (422), (333), and (440) crystallographic planes, which agree with those reported for the standard crystal structure of magnetite (Fe_3O_4).[28,33–36]

a)

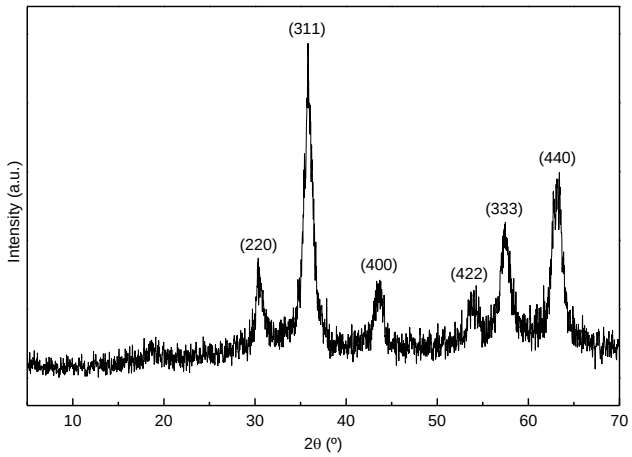

b)

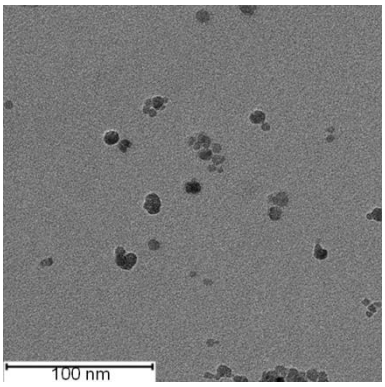

c)

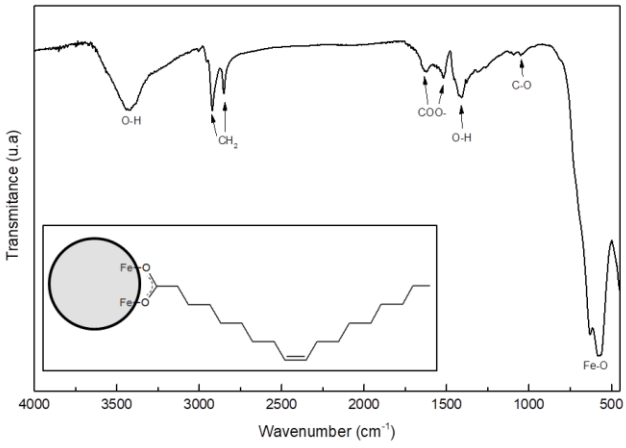

Figure 2. a) Wide-angle X-ray diffractogram, b) TEM image, and c) FTIR spectrum of the MNPs. The inset in (c) shows a scheme of the chelating bidentate interaction between the COO^- group of the oleic acid and iron atoms at the surface of the nanoparticle.

The crystal size (D) of the MNPs could be determined through Scherrer's equation:[37]

$$D = \frac{\kappa \cdot \lambda}{\beta \cdot \cos\theta} \quad (6)$$

where κ is the Scherrer constant (0.9), λ is the radiation wavelength (Cu Kα = 0.15418 nm), β is the width at half height of the selected peak in radians, and θ is Bragg angle.

According to this equation, and using the diffraction signal corresponding to the (311) crystallographic plane, the crystal size was calculated to be 7 nm. However, the "crystallite size" is not necessarily synonymous with "particle size" and this method is only an estimation of the diameter of the magnetite nanoparticles.[28]

The morphology of the MNPs was further analyzed by TEM. As can be observed in Figure 2b, the MNPs are spherical and they are well individualized. The average particle diameter of the MNP was calculated from TEM images by performing 80 measurements to be 8.0 ± 2.2 nm, which is in accordance with the estimated value by Scherrer's equation and also with the values reported in literature.[28,36,38]

FTIR spectroscopy was used to identify the interaction of oleic acid, which was used as a surface modifier, with the MNPs. As can be observed in Figure 2c, the bands associated with asymmetric and symmetric stretching vibration of C-H bonds in methylene groups[28,39,40] are present at 2921 and 2850 cm^{-1}, respectively. At 1622 and 1520 cm^{-1} the bands ascribed to asymmetric and symmetric carboxylate (COO^-) stretching vibrations, respectively, can be observed.[36,40–42] At 1415 cm^{-1} the band ascribed to coordinate in-plane deformation of the hydroxyl groups of the carbonyl group, i.e. oleic acid physisorbed on particle surface can be seen.[28,40] The band observed at 1050 cm^{-1} is related to C-O single bond stretching vibration after adsorption of the oleic acid on the particle surface.[28] The broad band centered at 582 cm^{-1} corresponds to Fe-O bonds of magnetite.[28,33,34] Finally, the broad band centered at 3420 cm^{-1} could be attributed to the O-H vibration of adsorbed water on the nanoparticles' surface.[40]

The wavenumber separation, Δ, between the asymmetric and symmetric COO- stretching vibration bands can be used to distinguish the type of the interaction between the carboxylate head and the metal atom, which can be monodentate (Δ = 200-300 cm^{-1}), bridging bidentate (Δ = 140-190 cm^{-1}), chelating bidentate (Δ < 100 cm^{-1}) and ionic interaction.[36,41,42] The Δ observed here (1622 - 1520 = 102 cm^{-1}) is ascribed to chelating bidentate denoting that the interaction between COO- group of oleic acid and the Fe is covalent[36] and thus oleic acid in carboxylate form is chemisorbed on the surface of oxide particles (Scheme inside Figure 2c).[40] These results revealed that

oleic acid was both physi- and chemisorbed onto the magnetite nanoparticles as a carboxylate.[28,36]

It is well known that the thermal transitions of the domains used for shape fixing and recovery play a key role in the context of shape-memory behavior and is important to define the shape memory test conditions, and also essential for developing an understand for the processes at play. Therefore the thermal behavior of the bionanocomposites was analyzed by DSC. In Figure 3 the heating and cooling traces of the neat PU and the bionanocomposites containing 3 or 5 wt% MNPs and also the LDI/PD and macrodiol building blocks are shown, while in Table 1 the thermal transitions and the relative crystallinity values are reported. As can be observed, the neat PU and the bionanocomposites show the thermal transitions associated with neat LDI/PD-rich and macrodiol-rich domains, indicating that the materials made show a microphase separated structure. The magnification of the low-temperature portion of the traces (Figure 3b) shows that the neat PU and the bionanocomposites show a T_g around -45 ºC and -44 and -42 ºC, respectively, which is ascribed to $T_{gMacrodiol}$. The increasing tendency of the T_g of the nanocomposites suggests that the MNPs interact with the macrodiol rich domains, restrict the chain mobility, and hence increase the T_g.[43] Moreover, at higher temperatures (-14; -11 and -12 ºC) the T_g associated with LDI/PD rich domain can be observed, which is slightly lower in the bionanocomposites. Furthermore, this glass transition is the T_{trans}, which would trigger the shape-memory of the bionanocomposites. In order to develop a better understanding of the interaction between the MNP and the macrodiol- and LDI/PD-rich domains, the solubility parameters of the macrodiol, LDI/PD, and oleic acid used for the synthesis of MNPs were calculated by Hoy's method.[44] The obtained theoretical parameters were 20.1, 24.3 and 18.5 $J^{1/2}$ $cm^{-3/2}$, respectively, denoting that the MNPs coated with oleic acid would preferably interact with macrodiol rich domain, which is in agreement with the DSC results.

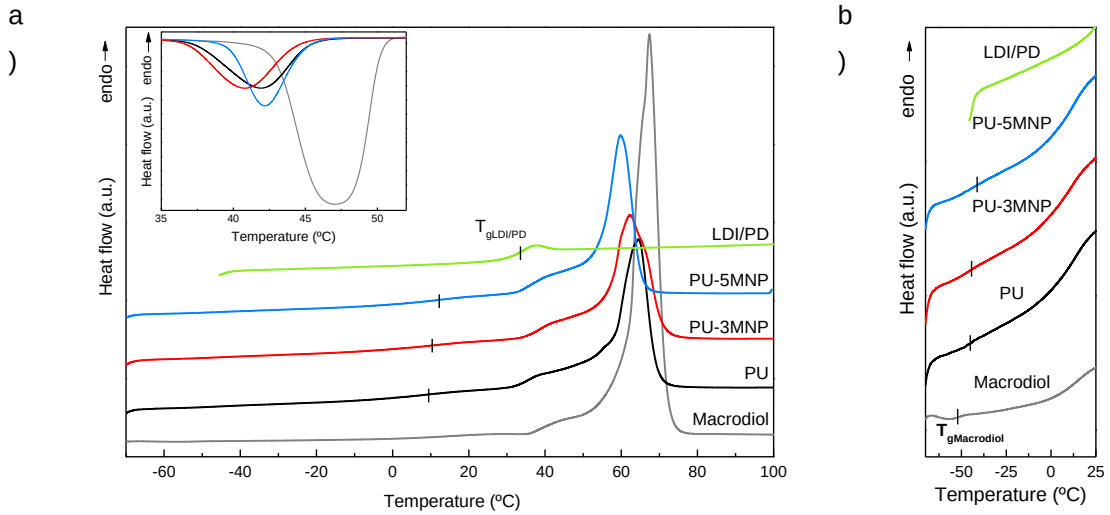

Figure 3. a) DSC heating traces of the neat PU and bionanocomposites with 3 or 5 wt% MNPs. The traces of the macrodiol and the LDI/PD building blocks are also shown. The inset shows the corresponding cooling traces. b) Magnification of the low-temperature portion of the traces shown in (a).

Table 1. Thermal characteristics and crystallinity values established of the neat PU and the bionanocomposites containing 3 or 5 wt% MNPs. Also shown are data for the LDI/PD and the macrodiol building blocks.

Sample	$T_{gMacrodiol}$ [a] (°C)	$T_{gLDI/PD}$ [a] (°C)	T_m [a] (°C)	ΔH_m [a] (J g^{-1})	T_c [a] (°C)	ΔH_c [a] (J g^{-1})	χ_c heating	χ_c cooling	T_α [b] (ºC)
Macrodiol	-52	-	70	142	46	-93	-	-	-
PU	-45	14	65	63	42	-59	1.00	1.00	19
PU-3MNP	-44	11	62	60	41	-56	0.97	0.98	22
PU-5MNP	-42	12	60	58	42	-55	0.97	0.98	22
LDI/PD	-	33	-	-	-	-	-	-	-

[a]Measured by DSC

[b]Measured by DMA

Finally, all DSC heating traces (except the one of the LDI/PD building block) show a sharp endothermic peak around 60 – 65 ºC, which is associated with melting of crystalline domains formed by the macrodiol. The PU-MNP bionanocomposites show slightly lower T_m, ΔH_m, and $\chi_{c\ heating}$ values than the neat PU, indicating that MNPs tend to preferably interact with macrodiol-rich domains and the addition of the MNPs decrease the crystallization ability of the macrodiol-rich domains a bit. This behavior was also observed in the cooling DSC thermograms, inset Figure 3a, where it was observed that

overall crystallinity and $\chi_{c\ cooling}$ decreases as the MNP content increases. Similar results were reported in the literature.[45]

Wide-angle XRD was used to analyze the crystallinity of PU-3MNP bionanocomposite. In Figure 4, the XRD patterns of PU-3MNP together with those of the macrodiol and PU are shown. Both PU and PU-3MNP show two strong peaks at 2θ angles that are similar to the peaks observed for the neat macrodiol. This fact denotes that the peaks observed are related to the crystallizable macrodiol-rich domains. However, the peak observed at 24.7° in the macrodiol shifts to a slightly lower angle, suggesting that different chains arrangements are formed.[46] Moreover, in PU-3MNP the crystallinity was lower than in the neat PU, since the intensity of the peak at 2θ = 21.4° decreases considerably. This fact suggests the tendency of the MNPs to interact with macrodiol-rich domain, which was also deduced from the results obtained by DSC and the calculation of the solubility parameters.

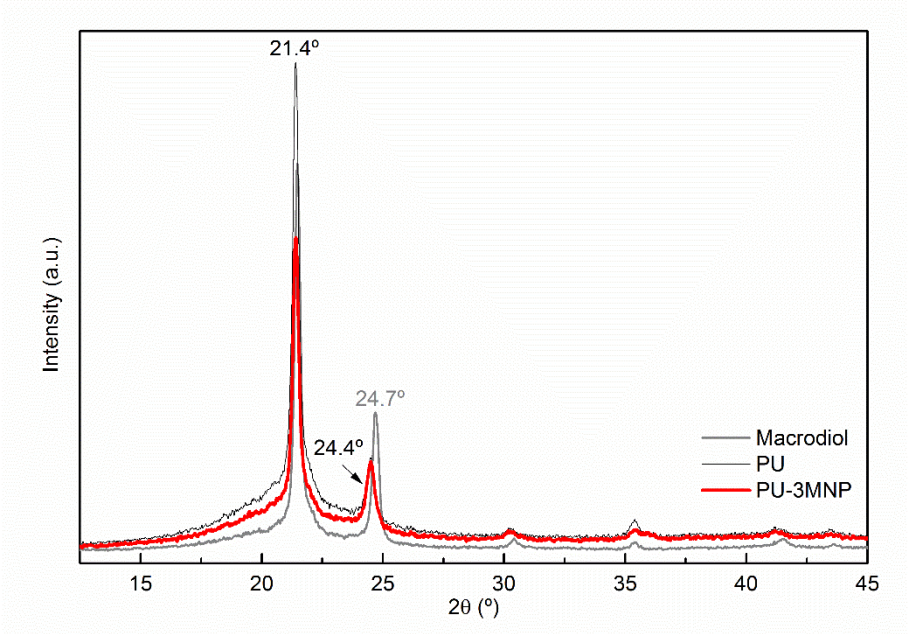

Figure 4. X-ray diffractogram of the neat PU, the bionanocomposite with 3 wt% MNPs, and the macrodiol building block.

The mechanical behavior of the PU and the PU-MNP bionanocomposites was analyzed by dynamic mechanical analysis (DMA). Figure 4 shows the temperature dependence of the storage modulus and the tanδ of all compositions. At low temperature, all materials are rigid, with a storage modulus (E') of 2360, 2700 and 2470 MPa at -75 ºC for PU, PU-3MNP, and PU-5MNP, respectively. At higher temperature a sharp decrease of E' and a simultaneous maximum in tanδ can be observed, which is related to the T_g of the LDI/PD rich domain.[10] In the rubbery state the E' continues gradually decreasing until at

temperatures around 60 °C a sharp decrease of E' occurs, which corresponds to the disruption of the crystalline structure of the material. In general, slightly higher E' values were observed for bionanocomposites, due to some reinforcement imparted by the MNPs, as observed by other authors.[9] Table 1 displays the maximum of tanδ and the values of this α transition temperature (T_α) seem not to be dependent of MNP content, since similar values were obtained for PU-3MNP and PU-5MNP.

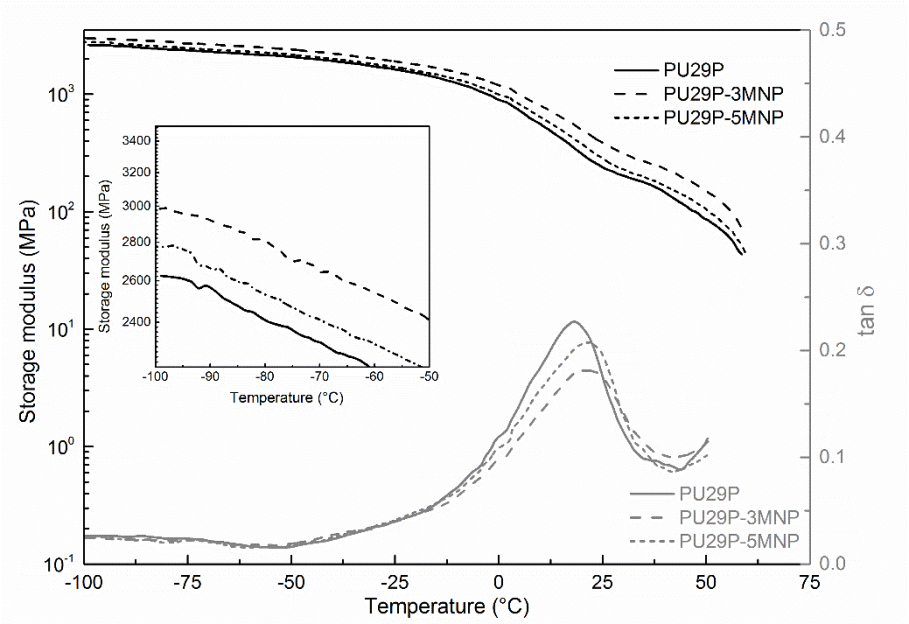

Figure 5. Storage modulus and loss factor of the neat PU and bionanocomposites with 3 or 5 wt% MNPs.

In order to analyze the effect of the addition of MNP on mechanical properties tensile tests were performed. The stress-strain curves of the bio-based polyurethane and PU-MNPs are shown in Figure 6, while in Table 2 the characteristic values derived from the curves are gathered. In our previous work[10] it was observed that the mechanical properties of the bio-based polyurethane matrix were governed by the crystallinity of the macrodiol-rich domains, and hence, the mechanical properties of the prepared bionanocomposites were not greatly affected by the incorporation of the nanoparticles. As previously deduced from DSC and solubility parameters, the MNPs tend to interact with the macrodiol-rich domains and they do not form a percolated network which could interfere in the strain of the bionanocomposite.[47] Furthermore, it can be surmised that the MNPs could be able to absorb strain energy upon deformation, acting as effective stress-bearing phase during deformation,[48,49] since the elastic modulus as well as stress at yield and at break are not affected in a great extent.

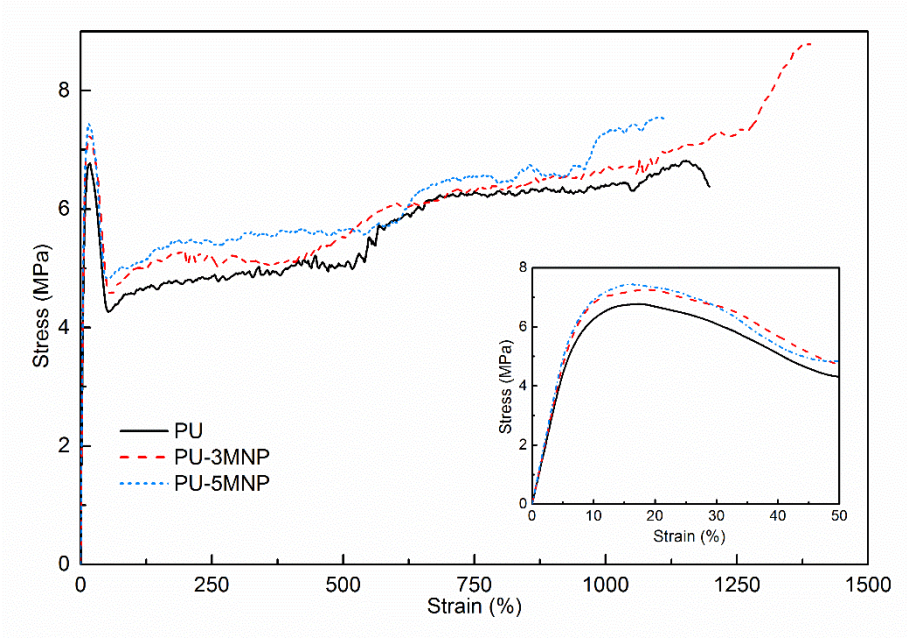

Figure 6. Stress-strain curves of the neat PU and bionanocomposites with 3 or 5 wt% MNPs.

Table 2. Mechanical properties of the neat PU and the bionanocomposites containing 3 or 5 wt% MNPs.

Sample	E (MPa)	σ_y (MPa)	σ_b (MPa)	ε_y (%)	ε_b (%)
PU	93 ± 8	6.9 ± 0.2	7.2 ± 0.4	16.9 ± 2.2	1149 ± 153
PU-3MNP	98 ± 1	7.1 ± 0.1	8.4 ± 0.8	15.8 ± 2.0	1342 ± 72
PU-5MNP	102 ± 4	7.3 ± 0.3	7.7 ± 0.1	16.3 ± 1.4	1105 ± 78

Measured by UTM at 25 °C

Since it was observed that the bio-based polyurethane matrix shows thermally activated shape-memory properties,[10] the influence of the addition of MNP on shape-memory properties was analyzed. In Table 3, the R_f and R_r values of five consecutive shape fix and release cycles of the neat PU and PU-MNP bionanocomposites are shown. In all cycles, the addition of MNPs results in a slightly higher shape fixity, which could be related, in analogy to findings reported by Ratna et al.[1] reported, to the higher E' in the glassy state. Nevertheless, high fixity (92-100%) is observed across the board, and generally, the fixity increases slightly from one cycle to the next. Since all prepared materials were stretched above their yield point, R_r values are in the first cycle lower than 100%. The previous analysis of the thermally activated shape-memory properties of the neat PU matrix revealed that the original shape was restored through crystalline structures,[10] as the residual stress introduced in the sample during the stretching could be stored in though physical crystalline segregated domains, which acts as the driving

force for shape recovery.[50–52] Regarding the shape recovery of the bionanocomposites, it can be observed that similar R_r values were obtained despite the slightly lower overall crystallinity of the bionanocomposites.

Moreover, the changes observed in both ratios, R_f and R_r, between the first cycle and the remaining cycles can be attributed to the history of the sample. During the first cycle, the reorganization of the polymer at molecular scale takes place, involving the redistribution in the direction of the stress.[7,53]

Table 3. R_f and R_r values established in five consecutive shape fix and release cycles of the neat PU and the bionanocomposites containing 3 or 5 wt%.

Cycle	PU		PU-3MNP		PU-5MNP	
	R_f (%)	R_r (%)	R_f (%)	R_r (%)	R_f (%)	R_r (%)
1	91.6	87.3	94.7	88.2	93.3	88.7
2	93.4	99.3	99.0	94.0	98.1	97.0
3	94.8	99.5	98.5	97.9	99.5	97.1
4	96.4	99.5	98.4	99.6	98.7	99.1
5	99.4	100.0	98.2	100.0	98.7	100.0

All of the bionanocomposites show magnetic behavior, which was qualitatively verified by approaching the bionanocomposites with a magnet; an example of the magnetic behavior of PU-5MNP is shown in Figure 7a. In addition, the magnetically activated release of a temporary shape programmed into a film of the PU-5MNP bionanocomposite was studied. To that end, the PU-5MNP bionanocomposite and the neat PU reference were exposed to an AMF. In Figure 7b and 7c the surface temperatures of the matrix and PU-5MNP during AMF excitation are shown. As can be observed, the temperature of the surface of PU-5MNP bionanocomposite increases immediately after the AMF excitation starts from 22 to 25 ºC, whereas, the profile of the surface temperature of the PU matrix remains almost constant. This behavior reflects that the MNPs are indeed able to increase the temperature of the bionanocomposite when an AMF is applied. Figure 7d shows the shape recovery of a fixed shape of PU-5MNP bionanocomposite while an AMF with a frequency of 1018 kHz is applied. The recovery of the original shape is fast and almost complete recovery of the original shape of the film is reached in about 14 s.

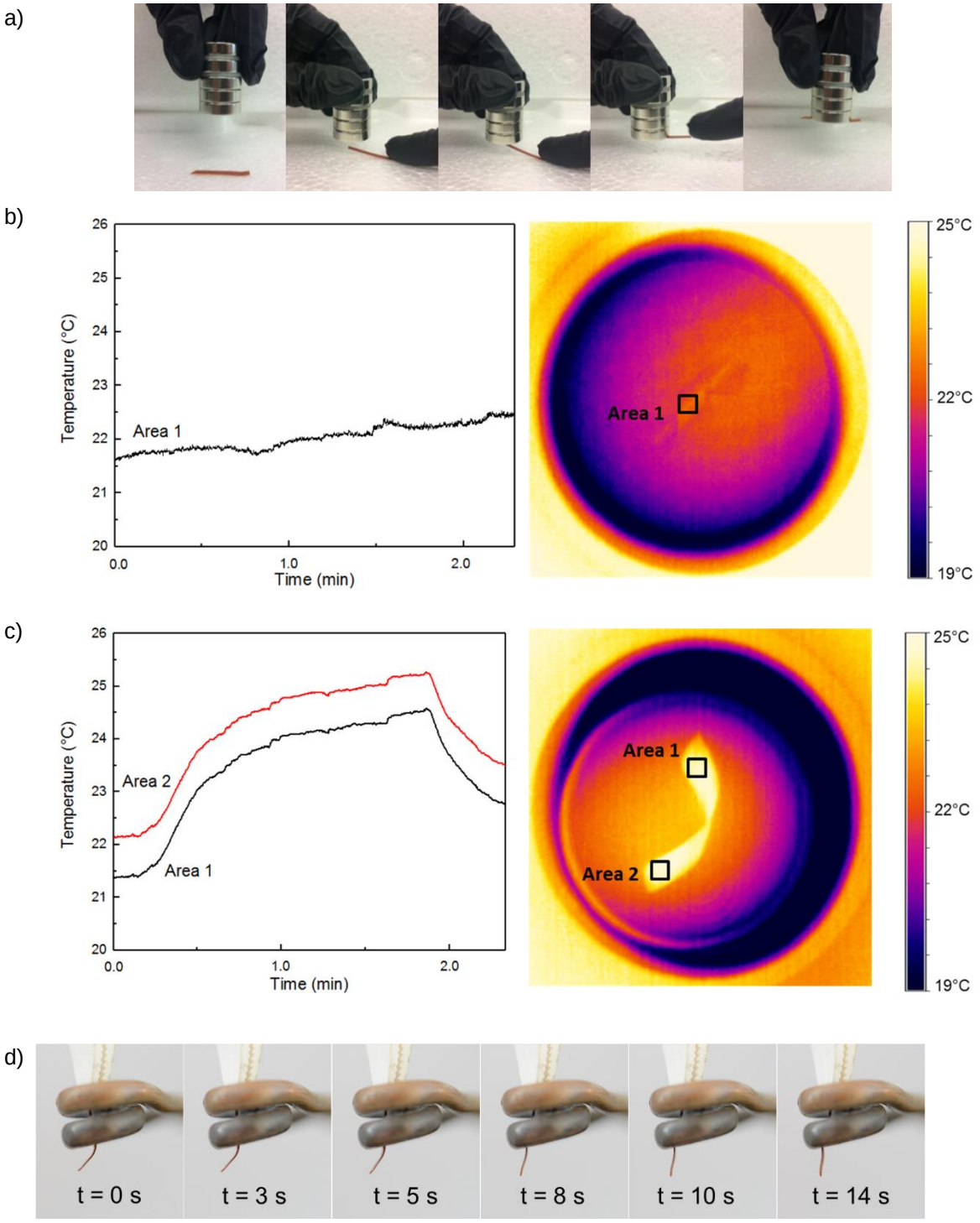

Figure 7. a) Magnetic response of PU-5MNP bionanocomposites. b) Surface temperature profile of the neat PU and c) the PU-5MNP bionanocomposites during alternating magnetic field excitation. d) Photographs documenting the magnetically activated shape recovery of the fixed shape of PU-5MNP bionanocomposite.

Thermo- and magneto- responsive shape-memory polyurethane bionanocomposites could be used for biomedical applications. In a previous study,[10] it was observed that the bio-based matrix showed a non-toxic behavior, according to performed short-term

cytotoxicity assays. Therefore, in light of the results obtained for the matrix, the in vitro biocompatibility of PU-3MNP bionanocomposite was also evaluated by performing short-term cytotoxicity, hemocompatibility and cell adhesion assays. The viability of PU-3MNP bionanocomposite (Figure 8a) is similar to the obtained from negative control and it is considerately higher than the established acceptance limit of 70% by ISO 10993-5 standard,[54] denoting that the material shows a non-toxic behavior. In order to determine the interaction of PU-3MNP with blood, the integrity of red blood cells membrane was analyzed following cyanomethemoglobin method. As can be observe in Figure 8b, the positive control produces complete lysis while for PU-3MNP the hemolysis is lower than 5%, indicating the hemocompatibility of the material. Furthermore, as can be seen in Figure 8c the hemolytic response of the bionanocomposite is negative due to the supernatant is colorless while for the positive control it is positive according to the red color of the supernatant. Finally, as can be observed in SEM images (Figure 8d), where the adhesion of cells to PU-3MNP bionanocomposites is shown, cells are well adhere to the surface. In addition, in more detailed view (enlarged image), it can be seen that cells acquire a flattened morphology and present numerous cytoplasmic projections that allows stable cell adhesion. Taking into account the obtained preliminary results, the prepared PU-3MNP is both biocompatible and hemocompatible.

a)

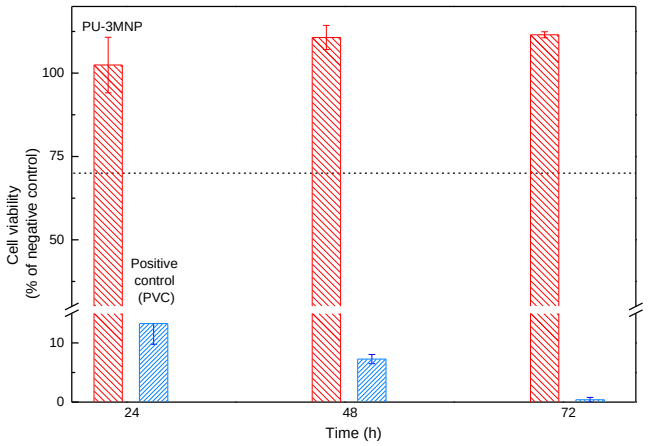

b)

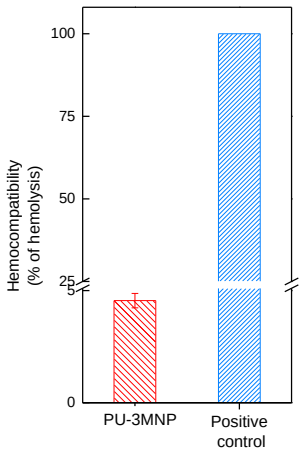

c)

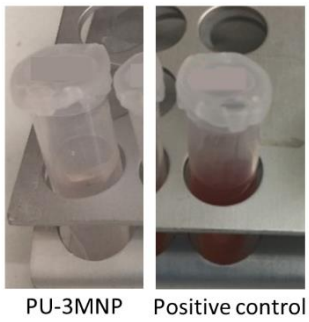

d)

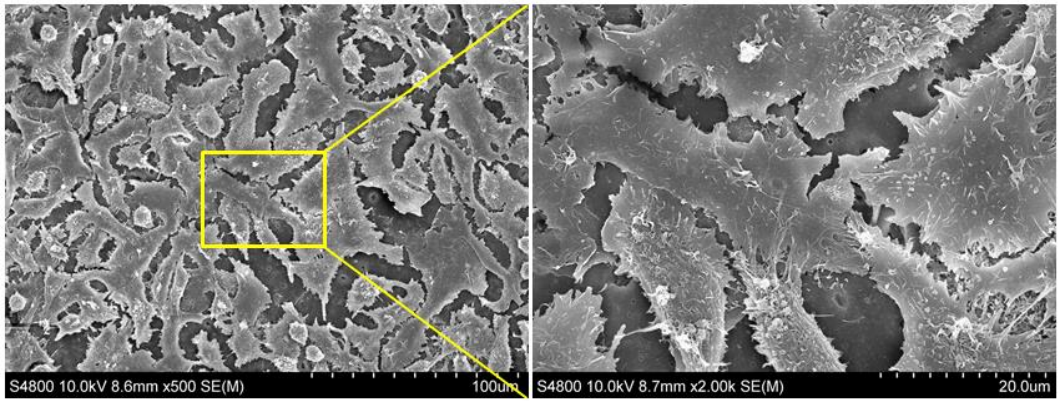

Figure 8. Evaluation of the biocompatibility of PU-3MNP bionanocomposite. a) In vitro cytotoxicity assay relative to negative control (the dash line represents the 70% of cell viability, b) percentage of hemolysis induced, c) digital image of the hemolytic response of PU-3MNP and positive control and d) SEM micrographs of L929 cultured on the surface of PU-3MNP after 72 h (left: 500X, right: 2000X).

CONCLUSIONS

Thermo- and magneto- responsive shape-memory bionanocomposites were prepared and characterized by using a bio-based polyurethane as matrix and different contents of MNP. The effect of the amount of magnetite nanoparticles on the final properties was analyzed. The MNPs tend to preferably interact with the macrodiol-rich crystalline

domains and slightly decrease the overall crystallinity. In addition, the mechanical properties of the bionanocomposites were not greatly affected by the presence of the MNPs. The addition of the MNPs increased the shape fixation capability slightly, especially in the first fixing cycle. The shape recovery was similar, despite the slightly lower crystallinity, suggesting that the MNPs were able to absorb strain energy upon deformation contributing to shape recovery. In addition, the bionanocomposites show magnetic behavior and they can be heated by an alternating magnetic field. In this way, the addition of MNPs allows fast and almost complete shape recovery via indirect triggering method without sacrifice the final properties of the matrix. Finally, taking into account the observed non-toxic behavior, good hemocompatibility and cell adhesion, the prepared magnetic bionanocomposites with MNP show potential to be used in further biomedical applications.

ACKNOWLEGMENTS

Financial support from the Basque Government (IT-776-13 and KK-2017/00003), the Spanish Ministry of Economy and Competitiveness (MAT2016-76294R), and the Adolphe Merkle Foundation is gratefully acknowledged. Furthermore, the authors wish to thank the “Macrobehavior-Mesostructure-Nanotechnology” SGIker unit from the University of the Basque Country for their technical support and Dr. Ana Alonso-Varona, Dr. Teodoro Palomares and Mrs. Patricia Garrido from the Department of Cellular Biology and Histology of the University of the Basque Country for the biocompatibility, hemocompatibility, and cell adhesion assays. T.C.-C. thanks the University of the Basque Country (DOCREC17/13).

REFERENCES

[1] D. Ratna, J. Karger-Kocsis, Recent advances in shape memory polymers and composites: a review, J. Mater. Sci. 43 (2008) 254–269.

[2] J. Leng, X. Lan, Y. Liu, S. Du, Shape-memory polymers and their composites: stimulus methods and applications, Prog. Mater. Sci. 56 (2011) 1077–1135.

[3] B.Q.Y. Chan, Z.W.K. Low, S.J.W. Heng, S.Y. Chan, C. Owh, X.J. Loh, Recent advances in shape memory soft materials for biomedical applications, Appl. Mater. Interfaces 8 (2016) 10070–10087.

[4] L. Sun, W.M. Huang, C.C. Wang, Y. Zhao, Z. Ding, H. Purnawali, Optimization of the shape memory effect in shape memory polymers, J. Polym. Sci. Part A Polym. Chem. 49 (2011) 3574–3581.

[5] M. Behl, A. Lendlein, Shape-memory polymers, Mater. Today 10 (2007) 20–28.

[6] X. Zheng, S. Zhou, X. Li, J. Weng, Shape memory properties of poly (D,L-lactide)/hydroxyapatite composites, Biomaterials 27 (2006) 4288–4295.

[7] A. Lendlein, S. Kelch, Shape-memory polymers, Angew. Chem. Int. Ed. 41 (2002) 2034–2057.

[8] P.T. Mather, X. Luo, I.A. Rousseau, Shape memory polymer research, Annu. Rev. Mater. Res. 39 (2009) 445–471.

[9] H. Zou, C. Weder, Y.C. Simon, Shape-memory polyurethane nanocomposites with single layer or bilayer oleic acid-coated Fe_3O_4 nanoparticles, Macromol. Mater. Eng. 300 (2015) 885–892.

[10] T. Calvo-Correas, A. Santamaria-Echart, A. Saralegi, L. Martin, Á. Valea, M.A. Corcuera, A. Eceiza, Thermally-responsive biopolyurethanes from a biobased diisocyanate, Eur. Polym. J. 70 (2015) 173–185.

[11] B.Q.Y. Chan, S.S. Liow, X.J. Loh, Organic – inorganic shape memory thermoplastic polyurethane based on polycaprolactone and polydimethylsiloxane, RSC Adv. 6 (2016) 34946–34954.

[12] B.Q.Y. Chan, S.J.W. Heng, S.S. Liow, K. Zhang, X.J. Loh, Dual-responsive hybrid thermoplastic shape memory polyurethane, Mater. Chem. Front. 1 (2017) 767–779.

[13] P. Singhal, W. Small, E. Cosgriff-Hernandez, D.J. Maitland, T.S. Wilson, Low density biodegradable shape memory polyurethane foams for embolic biomedical applications, Acta Biomater. 10 (2014) 67–76.

[14] A. Lendlein, R. Langer, Biodegradable, elastic shape-memory polymers for potential biomedical applications, Science 296 (2002) 1673–1676.

[15] H.M. Chen, L. Wang, S.B. Zhou, Recent progress in shape memory polymers for biomedical applications, Chinese J. Polym. Sci. 36 (2018) 905–917.

[16] M.A. Corcuera, L. Rueda, B. Fernandez-d'Arlas, A. Arbelaiz, C. Marieta, I.

Mondragon, A. Eceiza, Microstructure and properties of polyurethanes derived from castor oil, Polym. Degrad. Stab. 95 (2010) 2175–2184.

[17] C.S. Wang, D.J. Kenney, Effect of hard segments on morphology and properties of thermoplastic polyurethanes, J. Elastomers Plast. 27 (1995) 182–199.

[18] A. Gandini, The irruption of polymers from renewable resources on the scene of macromolecular science and technology, Green Chem. 13 (2011) 1061–1083.

[19] A. Gandini, T.M. Lacerda, From monomers to polymers from renewable resources: recent advances, Prog. Polym. Sci. 48 (2015) 1–39.

[20] M.A. Corcuera, A. Saralegi, B. Fernandez-d'Arlas, I. Mondragon, A. Eceiza, Shape memory polyurethanes based on polyols derived from renewable resources, Macromol. Symp. 321–322 (2012) 197–201.

[21] A. Saralegi, L. Rueda, B. Fernández-d'Arlas, I. Mondragon, A. Eceiza, M.A. Corcuera, Thermoplastic polyurethanes from renewable resources: effect of soft segment chemical structure and molecular weight on morphology and final properties, Polym. Int. 62 (2013) 106–115.

[22] M.L. Auad, T. Richardson, M. Hicks, M.A. Mosiewicki, M.I. Aranguren, N.E. Marcovich, Shape memory segmented polyurethanes: dependence of behavior on nanocellulose addition and testing conditions, Polym. Int. 61 (2012) 321–327.

[23] W. Wang, D. Liu, L. Lu, H. Chen, T. Gong, J. Lv, S. Zhou, The improvement of the shape memory function of poly(ε-caprolactone)/nano-crystalline cellulose nanocomposites via recrystallization under a high- pressure environment, J. Mater. Chem. A 4 (2016) 5984–5992.

[24] Y. Liu, Y. Li, G. Yang, X. Zheng, S. Zhou, Multi-stimulus-responsive shape-memory polymer nanocomposite network cross-linked by cellulose nanocrystals, Appl. Mater. Interfaces 7 (2015) 4118–4126.

[25] A. Saralegi, S.C.M. Fernandes, A. Alonso-Varona, T. Palomares, E.J. Foster, C. Weder, A. Eceiza, M.A. Corcuera, Shape-memory bionanocomposites based on chitin nanocrystals and thermoplastic polyurethane with a highly crystalline soft segment, Biomacromolecules 14 (2013) 4475–4482.

[26] T. Gong, W. Li, H. Chen, L. Wang, S. Shao, S. Zhou, Remotely actuated shape memory effect of electrospun composite nanofibers, Acta Biomater. 8 (2012)

1248–1259.

[27] G.D. Soto, C. Meiorin, D. Actis, P. Mendoza Zélis, M.A. Mosiewicki, N.E. Marcovich, Nanocomposites with shape memory behavior based on a segmented polyurethane and magnetic nanostructures, Polym. Test. 65 (2018) 360–368.

[28] C. Meiorin, D. Muraca, K.R. Pirota, M.I. Aranguren, M.A. Mosiewicki, Nanocomposites with superparamagnetic behavior based on a vegetable oil and magnetite nanoparticles, Eur. Polym. J. 53 (2014) 90–99.

[29] B. Wunderlich, Thermal analysis of polymeric materials, Springer, Berlin, 2005.

[30] I.O. for Standardization, ISO 10993-12:2007. Biological evaluation of medical devices. Part 12: Sample preparation and reference materials, (2007).

[31] International Organization for Standardization, ISO 10993-4:2009. Biological evaluation of medical devices. Part 4: selection of tests for interactions with blood, (2009).

[32] S.M. Chowdhury, S. Kanakia, J.D. Toussaint, M.D. Frame, A.M. Dewar, K.R. Shroyer, W. Moore, B. Sitharaman, In vitro hematological and in vivo vasoactivity assessment of dextran functionalized graphene., Sci. Rep. 3 (2013) 2584.

[33] R.A. Bini, R.F.C. Marques, F.J. Santos, J.A. Chaker, M. Jafelicci Jr., Journal of magnetism and magnetic materials synthesis and functionalization of magnetite nanoparticles with different amino-functional alkoxysilanes, J. Magn. Magn. Mater. 324 (2012) 534–539.

[34] L.A. Cobos Cruz, C.A. Martínez Perez, H.A. Monreal Romero, P.E. García Casillas, Synthesis of magnetite nanoparticles-b-cyclodextrin complex, J. Alloys Compd. 466 (2008) 330–334.

[35] Z. Es'haghzade, E. Pajootan, H. Bahrami, M. Arami, Facile synthesis of Fe_3O_4 nanoparticles via aqueous based electro chemical route for heterogeneous electro-Fenton removal of azo dyes, J. Taiwan Inst. Chem. Eng. 71 (2017) 91–105.

[36] L. Zhang, R. He, H.C. Gu, Oleic acid coating on the monodisperse magnetite nanoparticles, Appl. Surf. Sci. 253 (2006) 2611–2617.

[37] A.L. Patterson, The Scherrer formula for X-ray particle size determination, Phys. Rev. 56 (1939) 978–982.

[38] P. Guardia, B. Batlle-Brugal, A.G. Roca, O. Iglesias, M.P. Morales, C.J. Serna, A. Labarta, X. Batlle, Surfactant effects in magnetite nanoparticles of controlled size, J. Magn. Magn. Mater. 316 (2007) 756–759.

[39] D. Maity, S.G. Choo, J. Yi, J. Ding, J.M. Xue, Synthesis of magnetite nanoparticles via a solvent-free thermal decomposition route, J. Magn. Magn. Mater. 321 (2009) 1256–1259.

[40] M. González, I. Martín-Fabiani, J. Baselga, J. Pozuelo, Magnetic nanocomposites based on hydrogenated epoxy resin, Mater. Chem. Phys. 132 (2012) 618–624.

[41] H. Erdemi, A. Baykal, E. Karaoglu, M.S. Toprak, Synthesis and conductivity studies of piperidine-4-carboxylic acid functionalized Fe_3O_4 nanoparticles, Mater. Res. Bull. 47 (2012) 2193–2199.

[42] E. Karaoglu, A. Baykal, M. Senel, H. Sözeri, M.S. Toprak, Synthesis and characterization of piperidine-4-carboxylic acid functionalized Fe_3O_4 nanoparticles as a magnetic catalyst for Knoevenagel reaction, Mater. Res. Bull. 47 (2012) 2480–2486.

[43] X. Yan, Q. He, X. Zhang, H. Gu, H. Chen, Q. Wang, L. Sun, S. Wei, Z. Guo, Magnetic polystyrene nanocomposites reinforced with magnetite nanoparticles, Macromol. Mater. Eng. 299 (2014) 485–494.

[44] D.W. van Krevelen, “Properties of polymers,” Elsevier Scientific Publising Co., Amsterdam, 1990.

[45] M. Shahrousvand, M.S. Hoseinian, M. Ghollasi, A. Karbalaeimahdi, A. Salimi, F.A. Tabar, Flexible magnetic polyurethane/Fe_2O_3 nanoparticles as organic-inorganic nanocomposites for biomedical applications: properties and cell behavior, Mater. Sci. Eng. C. 74 (2016) 556–567.

[46] S. Taheri, G.M.M. Sadeghi, Microstructure–property relationships of organo-montmorillonite/polyurethane nanocomposites: influence of hard segment content, Appl. Clay Sci. 114 (2015) 430–439.

[47] N. Lin, S. Wei, T. Xia, F. Hu, J. Huang, A. Dufresne, Green bionanocomposites from high-elasticity “soft” polyurethane and high-crystallinity “rigid” chitin nanocrystals with controlled surface acetylation, RSC Adv. 4 (2014) 49098–49107.

[48] M. Charlon, B. Heinrich, Y. Matter, E. Couzigné, B. Donnio, L. Avérous, Synthesis, structure and properties of fully biobased thermoplastic polyurethanes, obtained from a diisocyanate based on modified dimer fatty acids, and different renewable diols, Eur. Polym. J. 61 (2014) 197–205.

[49] L. Hojabri, X. Kong, S.S. Narine, Functional thermoplastics from linear diols and diisocyanates produced entirely from renewable lipid sources, Biomacromolecules 11 (2010) 911–918.

[50] C.P. Buckley, C. Prisacariu, A. Caraculacu, Novel triol-crosslinked polyurethanes and their thermorheological characterization as shape-memory materials, Polymer 48 (2007) 1388–1396.

[51] C.M. Yakacki, R. Shandas, D. Safranski, A.M. Ortega, K. Sassaman, K. Gall, Strong, tailored, biocompatible shape-memory polymer networks, Adv. Funct. Mater. 18 (2008) 2428–2435.

[52] X.L. Wu, S.F. Kang, X.J. Xu, F. Xiao, X.L. Ge, Effect of the crosslinking density and programming temperature on the shape fixity and shape recovery in epoxy-anhydride shape-memory polymers, J. Appl. Polym. Sci. 131 (2014) 40559.

[53] B. Fernández-d'Arlas, J.A. Ramos, A. Saralegi, M. Corcuera, I. Mondragon, A. Eceiza, Molecular engineering of elastic and strong supertough polyurethanes, Macromolecules 45 (2012) 3436–3443.

[54] International Organization for Standardization, ISO 10993-5. Biological evaluation of medical devices. Test for in vitro cytotoxicity, (2009).

Abbreviations

SMPs: Shape-memory polymers

T_{trans}: Transition temperature

T_s: Switching temperature

STPUs: Segmented thermoplastic polyurethanes

LDI: L-lysine diisocyanate

PD: 1,3-propanediol

MNPs: Magnetite nanoparticles

AMF: An alternating magnetic field

THF: Tetrahydrofuran

ATCC : American Type Culture Collection

MEM: Minimum Essential Medium (MEM

FBS: Fetal bovine serum

R_f: shape fixity

R_r:Shape recovery

PFH: Plasma free hemoglobin

TBH: Total blood hemoglobin

TBHd: Diluted total blood hemoglobin

Δ: Wavenumber separation

T_α: α transition temperature